Applied Geochemistry 120 (2020) 104665

Contents lists available at ScienceDirect

Applied Geochemistry

journal homepage: http://www.elsevier.com/locate/apgeochem

Effects of basic intrusions on REE mobility of sandstones and their geological significance: A case study from the Qianjiadian sandstone-hosted uranium deposit in the Songliao Basin

Hui Rong [a,*], Yangquan Jiao [a], Xiaofeng Liu [a,**], Liqun Wu [a], Junmin Jia [a], Minqiang Cao [b]

[a] Key Laboratory of Tectonics and Petroleum Resources (China University of Geosciences), Ministry of Education, Wuhan, 430074, China
[b] Development Company of New Energy Sources of Liaohe Petroleum Exploration Bureau, CNPC, Panjin, 124010, China

ARTICLE INFO

Editorial handling by Prof. M. Kersten

Keywords:
REE mobility
Carbonate cements
Sandstones
Diabase dikes
Songliao basin

ABSTRACT

REE geochemistry of sandstones and their carbonate cements from the Upper Cretaceous Yaojia Formation in the Qianjiadian uranium deposit, southern Songliao Basin are illustrated in order to reveal effects of basic intrusions on REE mobility of sandstones and their geological significance. Compared with the sandstones far away from the diabase dikes, the sandstones near the diabase dikes are obviously depleted in REEs. ∑LREE content, ∑HREE content and ∑REE content all increase with an increase of the distance away from the diabase dikes. Carbonate cements in the sandstones comprise of dolomite, siderite, ankerite and calcite, which are successively formed from the early to late stage. In the sandstones near the diabase dikes, the dolomite and siderite are partly dissolved, and the ankerite is accumulated. ΣLREE content and ΣHREE content are both gradually decreasing in turn from the dolomite, to siderite, to ankerite, and to calcite. Dolomite content is positively correlated with ∑HREE content, siderite content is positively correlated with ∑LREE content or ∑HREE content, and ankerite content is inversely correlated with ∑LREE content. Dissolution of the dolomite and siderite and formation of the ankerite were aroused by intrusion of the diabase dikes, resulting in the sandstones near the diabase dikes being depleted in REEs. The study suggests that high-grade uranium mineralization may be attributed to the diabase dikes, REE depletion of the sandstones can be severe as a new prospecting indicator, and sandstones affected by igneous intrusions should be avoided during sampling for sandstone provenance by REEs.

1. Introduction

Magmatic activities in sedimentary basins have always been considered as a critical geologic factor affecting hydrocarbon generation, migration and accumulation, and metallic enrichment and mineralization (Einsele et al., 1980; Othman et al., 2001; Smith and Davies, 2006; Liu et al., 2015; Sliwinski et al., 2016; Zhang et al., 2016). Well documented studies have been focused on influences of igneous intrusions on diagenesis, mineral composition and reservoir properties of sandstones (Brauckmann and Fuchtbauer, 1983; Girard and Nahon, 1989; Summer and Ayalon, 1995; Ros, 1998; Mc Kinley et al., 2001; Grove, 2014; Grove et al., 2017). REEs have been served as indicators of petrogenesis and fluid geochemistry reflecting sedimentary history and diagenetic process of sandstones (McLennan and Taylor, 1979; Bhatia, 1985; Cuney and Mathieu, 2000; Chen et al., 2007; Tanaka et al., 2007; Xue et al., 2010). However, there is still little knowledge about geochemical behaviours of REEs within sandstones reformed by igneous intrusions. Carbonate cements serving as most common authigenic minerals in sandstones are very sensitive to diagenetic fluids, and are extremely soluble or precipitated (Kantorowicz et al., 1987; Chowdhury and Noble, 1996; Wang et al., 2010; Liu et al., 2014). There have been many studies focusing on tracing diagenetic fluids by using carbonate cements or evaluating effects of carbonate cements on reservoir heterogeneity (Beitler et al., 2005; Liu et al., 2011; Ma et al., 2016; Vincent et al., 2018; Lai et al., 2019), but little attention has been paid to relationship between carbonate cements and geochemical behaviours of REEs in sandstones, directly affecting reliability of application of REEs to trace sedimentary history and diagenetic process of sandstones.

In recent years, the Qianjiadian uranium deposit serving as a large sandstone-hosted uranium deposit has been found in the Upper

* Corresponding author.
** Corresponding author.
E-mail addresses: ronghui0411@163.com (H. Rong), xfliu@cug.edu.cn (X. Liu).

https://doi.org/10.1016/j.apgeochem.2020.104665
Received 30 November 2019; Received in revised form 22 May 2020; Accepted 2 June 2020
Available online 11 July 2020
0883-2927/© 2020 Elsevier Ltd. All rights reserved.

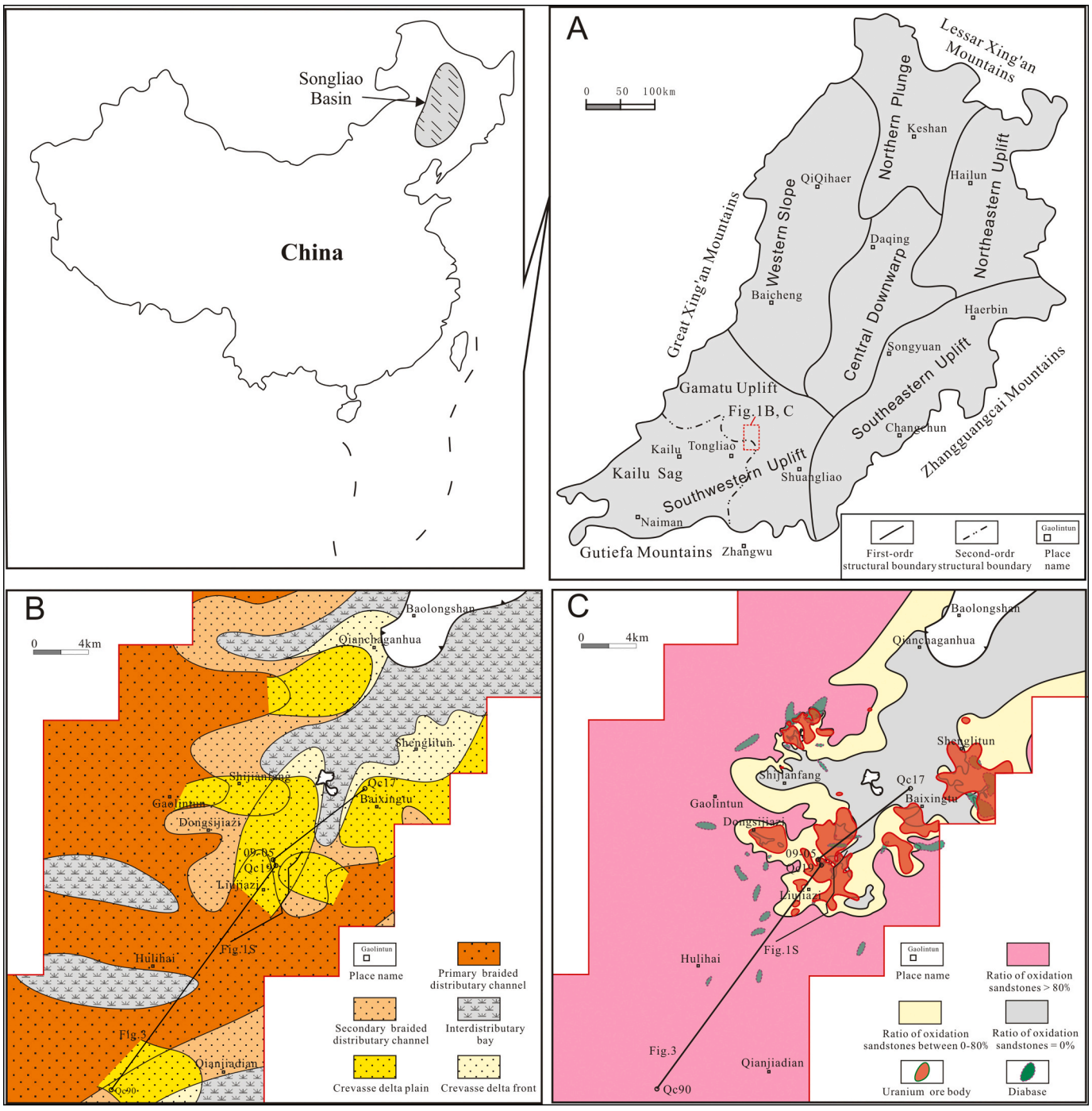


Fig. 1. (A) Tectonic units of the Songliao Basin (modified from Feng et al., 2010). (B) Sedimentary microfacies map of the lower part of the Yaojia Formation in the Qianjiadian uranium deposit (modified from Jiao et al., 2015). (C) Spatial distribution of the interstratified oxidation and diabases in the Qianjiadian uranium deposit; the data of the interstratified oxidation obtained from 880 drill holes referring to the lower part of the Yaojia Formation; the ratio of oxidized sandstones = (thickness of red sandstones and yellow sandstones/cumulative thickness of sandstones) * 100%; the data of the diabases also from 880 drill holes referring to all drilled strata mainly including the Qingshankou Formation, Yaojia Formation and Nenjiang Formation. (For interpretation of the references to color in this figure legend, the reader is referred to the Web version of this article.)

Cretaceous Yaojia Formation in the Songliao Basin (Jiao et al., 2015; Rong et al., 2016; Zhao et al., 2018). Sandstones of the Yaojia Formation are primarily composed of red sandstones and grey sandstones with a few yellow sandstones (Chen et al., 2008; Pang et al., 2010; Rong et al., 2016, 2019; Zhao et al., 2018). Lots of diabase dikes are widely distributed in the Qianjiadian uranium deposit (Luo et al., 2007, 2012; Xia et al., 2010; Rong et al., 2019). The diabase dikes are emplaced at 49.5 ± 5 Ma according to Ar–Ar dating (Xia et al., 2010) and always intrude into sandstones of the Yaojia Formation (Rong et al., 2019). Maximum burial depth of the Yaojia Formation in the Qianjiadian uranium deposit was less than 500 m (Tian et al., 2001; Li et al., 2008), diagenesis of these sandstones are relatively simple (Chen et al., 2008; Pang et al., 2010; Jia et al., 2018; Rong et al., 2016; Zhao et al., 2018), and complete cores from drill holes have been preserved, providing a convenient condition to study effects of igneous intrusions on geochemical behaviours of REEs of sandstones.

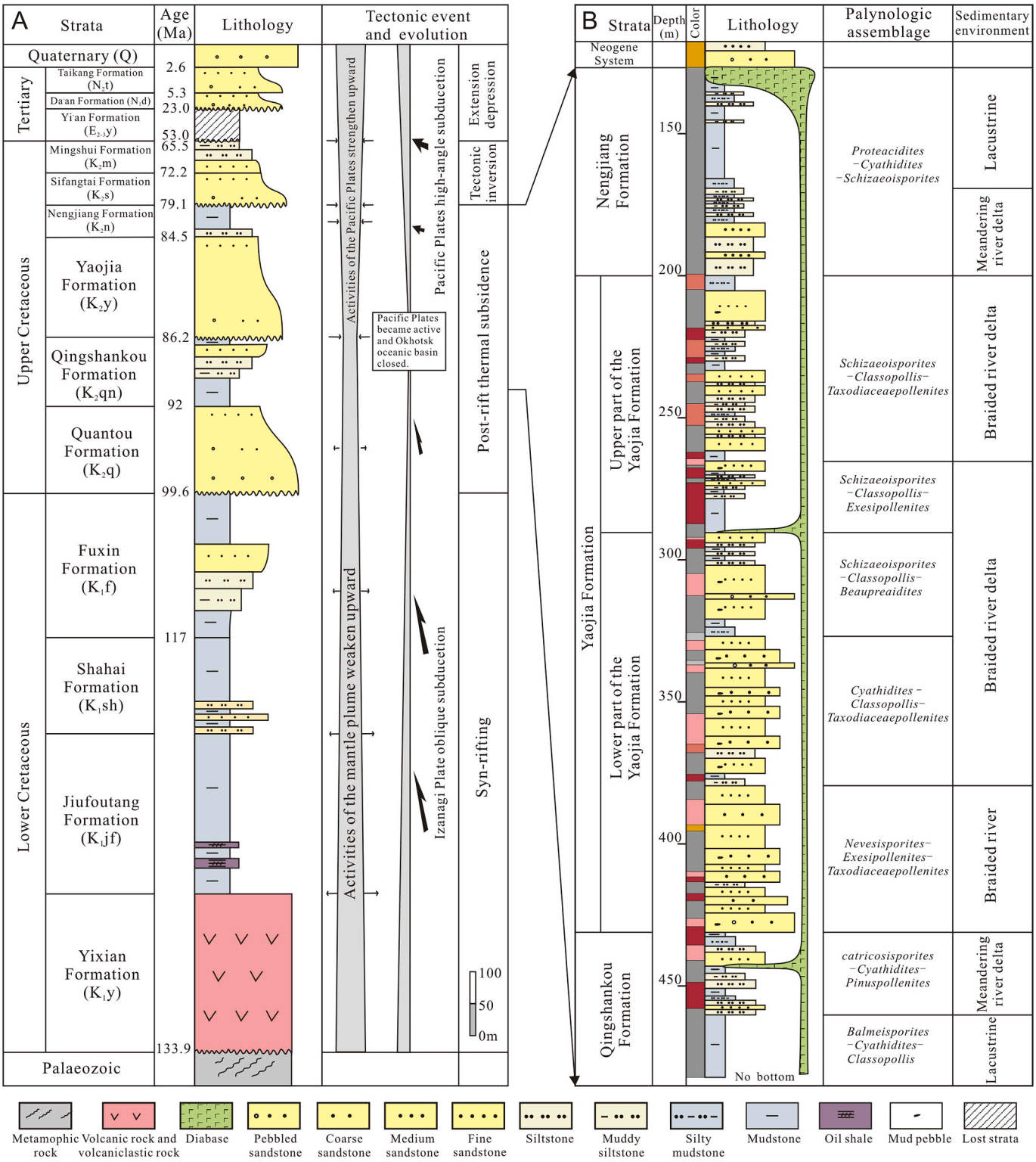


Fig. 2. (A) Stratigraphic column illustrating the stratigraphic architecture, lithologies and structure phase of the southern Songliao Basin (modified from Xu and Li, 1995 and Du et al., 2011). The Cretaceous and Cenozoic ages are cited from Huang et al. (2011) and Wan et al. (2013). The Yi'an Formation primarily distributed in the northwestern Songliao Basin was lost in the southern Songliao Basin (Fang et al., 2007). (B) Stratigraphic architecture of the Yaojia Formation in the Qianjiadian uranium deposit (Rong et al., 2016).

The aims of this paper is to characterize REE geochemistry of sandstones, occurrence and REE geochemistry of carbonate cements in sandstones from the Yaojia Formation in the Qianjiadian uranium deposit. According to these data, relationship between the REE mobility and carbonate cements of sandstones will be established, and effects of basic intrusions on REE mobility of sandstones and their geological significance will be discussed.

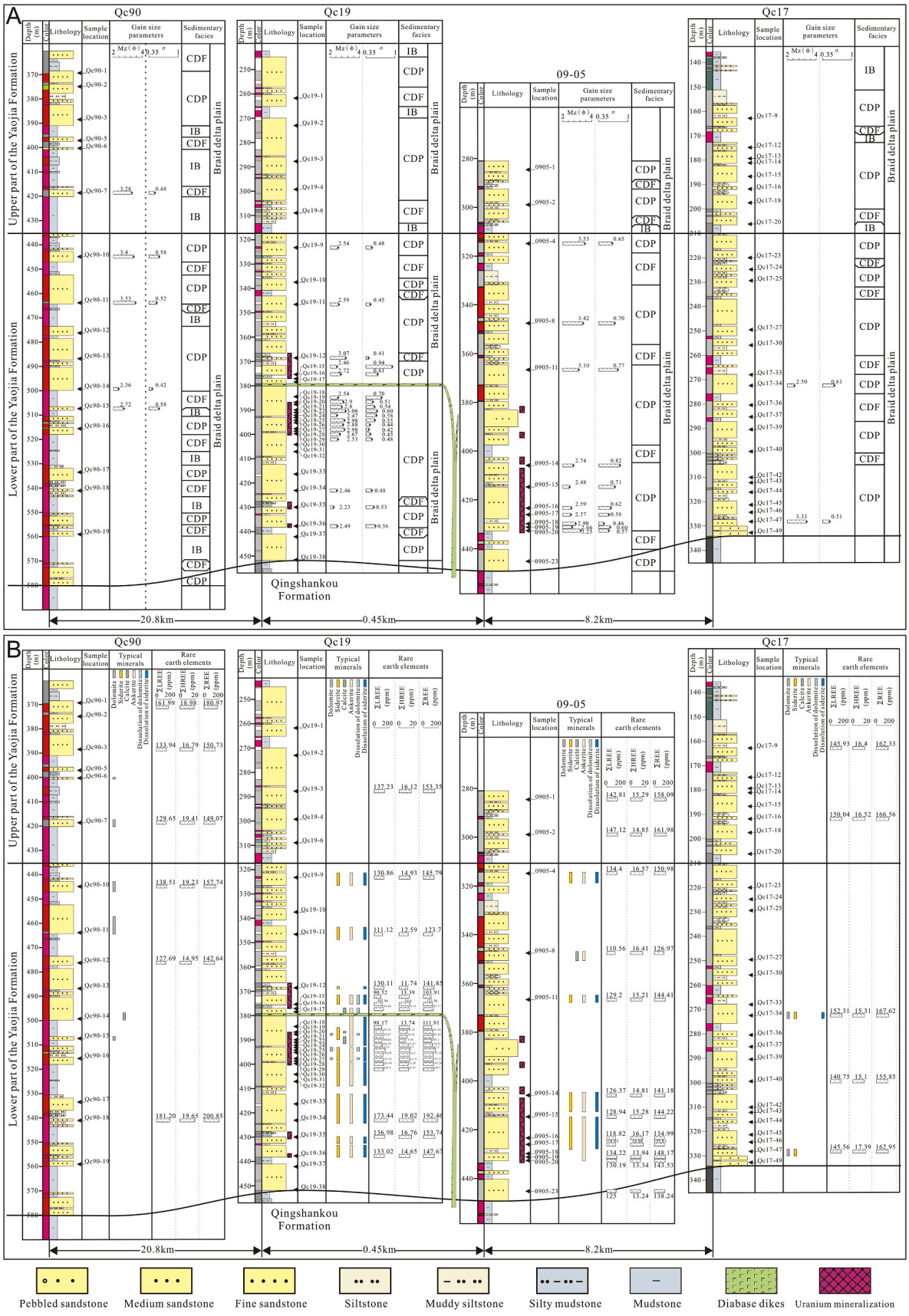


Fig. 3. Sample locations, grain size parameters, sedimentary facies, REEs and typical minerals from the four representative drill holes in the Qianjiadian uranium deposit. This figure illustrates that the sandstones near the diabase dikes are obviously depleted in REEs, and the dissolution of dolomite and siderite tends to occur in the sandstones near the diabase dikes. Locations of the four drill holes were shown in Fig. 1B, C.

		Lithology			
		Red sandstones far away from diabase dikes	Sandstones near diabase dikes		Grey sandstones far away from diabase dikes
			Red sandstones	Grey sandstones	
Typical drill holes		Qc90	Qc19 and 09-05		Qc17
Rare earth elements	∑REE^{A} (ppm)	162.99	136.18	139.49	163.62
	LREE^{A} (ppm)	145.34	121.15	125.36	146.60
	HREE^{A} (ppm)	17.65	15.03	14.14	17.02
Grain-size parameters	Mz ^{A}	2.72	2.98	2.76	2.92
	σ ^{A}	0.50	0.59	0.58	0.56
Carbonate cements	Dolomite (%)	4.5	0	0.2	1.1
	Siderite (%)	0	2.3	2.3	2.8
	Ankerite (%)	0	3.7	3.4	0
	Calcite (%)	0.9	0.7	0.4	0
	Dissolution of dolomite				
	Dissolution of siderite				

Fig. 4. Concentrations of ∑REE, ∑LREE and ∑HREE, ∑LREE/∑HREE, grain size parameters, and contents and morphology of carbonate cements in the sandstones from the Yaojia Formation in the Qianjiadian uranium deposit. ∑REE ^{A} represents the arithmetic average of the REE content of all samples in each zone, and ∑LREE ^{A}, ∑HREE ^{A}, ∑LREE/∑HREE ^{A}, La_N/Yb_N, La_N/Sm_N, and Gd_N/Yb_N are obtained the same as ∑REE ^{A}. Refer to Table 1S, 2S, 3S (Supplementary Material) for detailed data.

2. Geological background

The Songliao Basin, one of the most important energy-producing provinces in northeastern China, is surrounded by the Zhangguangcai Mountains to the east, Gutiefa Hill to the south, Great Xing'an Mountains to the west, and Lessar Xing'an to the north (Feng et al., 2010; Du et al., 2011; Wang et al., 2013, Fig. 1). The Qianjiadian uranium deposit is located across the Kailu Sag and Gamatu Uplift within the southeastern uplift of the Songliao Basin (Fig. 1).

The southern Songliao Basin underlain by basement of Palaeozoic metamorphic and magmatic rocks contains more than 5000m thick Cretaceous, Paleogene and Neogene clastic deposits (Fig. 2; Xu and Li, 1995). Four stages of tectonic evolution of the southern Songliao Basin have been recognized: syn-rifting in the Lower Cretaceous, post-rift thermal subsidence in the early stage of the Upper Cretaceous, basin inversion in the late stage of the Upper Cretaceous and extension depression in the Tertiary (Fig. 2; Feng et al., 2010; Du et al., 2011). The Lower Cretaceous deposits include the Yixian Formation (K_1y), Jiufotang Formation (K_1jf), Shahai Formation (K_1sh) and Fuxin Formation (K_1f) (Fig. 2). The Yixian Formation is characterized by volcanic and volcaniclastic rocks, whereas the others are composed of deltaic and lacustrine sediments. The Upper Cretaceous deposits are comprised of the Quantou Formation (K_2q), Qingshankou Formation (K_2qn), Yaojia Formation (K_2y) and Nenjiang Formation (K_2n) (Fig. 2). The Quantou Formation and Yaojia Formation primarily consist of fluvial and deltaic coarse-grained deposits, whereas the Qingshankou Formation and Nenjiang Formation contain the majority of lacustrine and deltaic fine-grained deposits (Fig. 2; Du et al., 2011). The Sifangtai Formation (K_2s) and Mingshui Formation (K_2m) are mainly composed of alluvial and fluvial coarse-grained deposits (Fig. 2; Du et al., 2011). The upper part of the basin is filled by the Tertiary and Quaternary fluvial deposits (Fig. 2; Du et al., 2011).

This study deals with the Upper Cretaceous Yaojia Formation which primarily consist of thick-bedded sandstones with a few thin-bedded mudstones (Fig. 2B). The widely-distributed sandstones in the Qianjiadian area vary in specific accumulation area: red and yellow ones in the southwest; grey ones in the northeast (Fig. 1C and S (Supplementary Material)). Diabase dikes with a thickness of 0.2–50m always intruded into the Yaojia Formation, or were often overlain by the Nenjiang Formation in the Qianjiadian uranium deposit (Figs. 1S and 2S (Supplementary Material); Rong et al., 2019). Sandstones of the Yaojia Formation near the diabase dikes have more carbonate cements and veins of pyrite than that far away from the diabase dikes (Fig. 2S (Supplementary Material)).

3. Material and methods

Four drill holes including Qc90, Qc19, 0905 and Qc17 in the Qianjiadian area have been selected for detailed study. Qc90 is far away from the diabase dikes and primarily composed of red sandstones, Qc19 and 0905 are near the diabase dikes and mainly consist of grey sandstones as well as a few red sandstones, and Qc17 is far away from the diabase dikes and primarily includes grey sandstones (Figs. 1C and 3). 0.4m thick diabase dikes intruded into the lower part of the Yaojia Formation from Qc19. Sample locations were shown in Fig. 3 and the samples were examined mainly by a set of tests including thin-section petrographic characterization, mineral morphology and identification, grain-size analysis, petrographic image analysis and bulk-rock and in-situ REE analysis.

Scanning electron microscope (SEM) analysis was conducted by the ZISS EVO LS15 equipment at Key Laboratory of Tectonics and Petroleum Resources (China University of Geosciences), Ministry of Education. Grain-size analysis of sandstones was carried out as follows: (1) Grain maximum apparent diameters were measured in the scaled photomicrographs by the Image-Pro Plus 6.0, ensuring a statistical number of grains of more than 200. (2) Grain maximum apparent diameters were transformed to sieving diameters by the calibration equation (Friedman, 1958, 1962) $D_i = 0.9027D_o + 0.3815$, where D_o = maximum apparent diameter (Φ) and D_i = sieving diameter (Φ). (3) Grain-size parameters of samples were calculated through a graphical method (Folk and Ward, 1957), where M_z = graphic mean grain size, and σ = standard deviation. The standard deviation (σ) can quantitatively represent the degree of

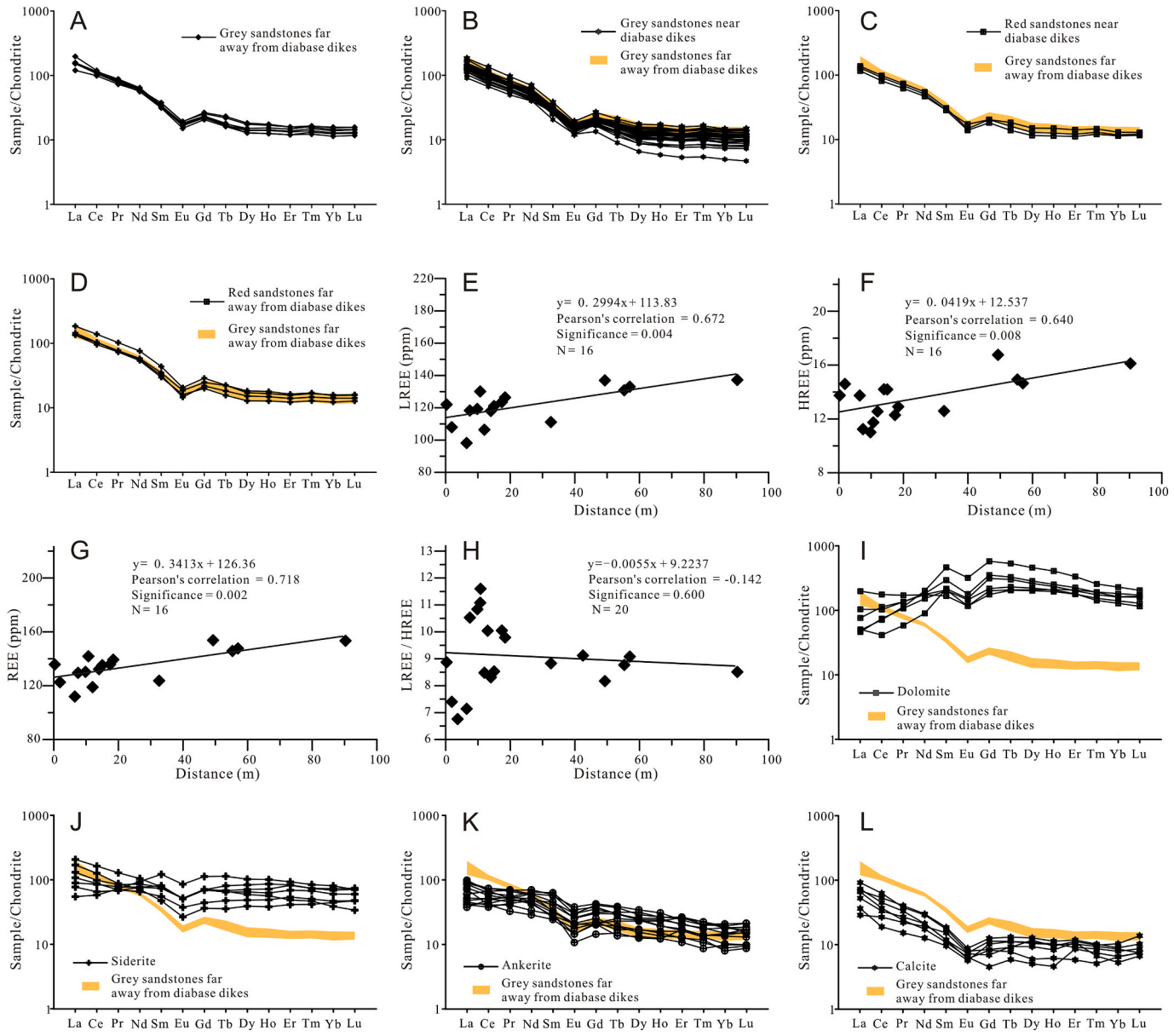


Fig. 5. (A) Chondrite-normalized REE patterns of the grey sandstones far away from the diabase dikes. (B) Chondrite-normalized REE patterns of the grey sandstones near the diabase dikes. (C) Chondrite-normalized REE patterns of the red sandstones near the diabase dikes. (D) Chondrite-normalized REE patterns of the red sandstones far away from the diabase dikes. (E) Cross-plot of the distance away from the diabase dikes against LREE of the sandstones in the drill of Qc19. (F) Cross-plot of the distance away from the diabase dikes against HREE of the sandstones in the drill of Qc19. (G) Cross-plot of the distance away from the diabase dikes against REE of the sandstones in the drill of Qc19. (H) Cross-plot of the distance away from the diabase dikes against LREE/HREE of the sandstones in the drill of Qc19. (I) Chondrite-normalized REE patterns of the dolomite. (J) Chondrite-normalized REE patterns of the siderite. (K) Chondrite-normalized REE patterns of the ankerite. (L) Chondrite-normalized REE patterns of the ankerite. Refer to Tables 1S and 3S (Supplementary Material) for detailed data. Chondrite normalizing values are from Sun and McDonough (1989). (For interpretation of the references to color in this figure legend, the reader is referred to the Web version of this article.)

sorting of the grains (Folk and Ward, 1957). Content of carbonate cements in sandstones is evaluated as follows: (1) Choose at least 3 representative scaled back-scattered electron images for each sample in a thin-section under the SEM equipped with EDS (Fig. 3S (Supplementary Material)). (2) Draw contours of carbonate cements and pack them with a selected color (Fig. 3S (Supplementary Material)). (3) Area percent of carbonate cements in back-scattered electron images are measured by software named Image-Pro Plus 6.0. So, content of carbonate cements is average area percent of carbonate cements in back-scattered electron images selected for each sample.

43 samples were analyzed for bulk-rock REEs at the Institute of Oceanology, Chinese Academy of Sciences, by ICP-MS ELAN DRC II. Bulk-rock REEs were analyzed at the Institute of Oceanology, Chinese Academy of Sciences, by ICP-MS ELAN DRC II. The samples were dried at 65 °C and 105 °C to completely dry, then were milled to less than 200 μm. These powders were weighed to 40 mg exactly, each in Teflon vials. Then 2 ml HF and 0.5 ml HNO_3 were added in turn and left to rest for 2 h then heated at 150 °C for 24 h on an electrothermal plate. Later, 0.25 ml $HClO_4$ was added, and samples were dried at 150 °C. When they were almost dry, 1 ml HNO_3 and 1 ml H_2O (18.2 MΩ) were added, then heated again on the electrothermal plate at 120 °C for 12 h. The final solution was diluted to about 40 g with H_2O (18.2MΩ) for ICP-MS analysis.

In-situ microanalysis of REEs of carbonate cements in sandstones was analyzed by LA-ICP-MS at the Wuhan Sample Solution Analytical Technology Co., Ltd., Wuhan, China. The detailed operating steps were referred to Zong et al. (2017). Laser sampling was performed using a

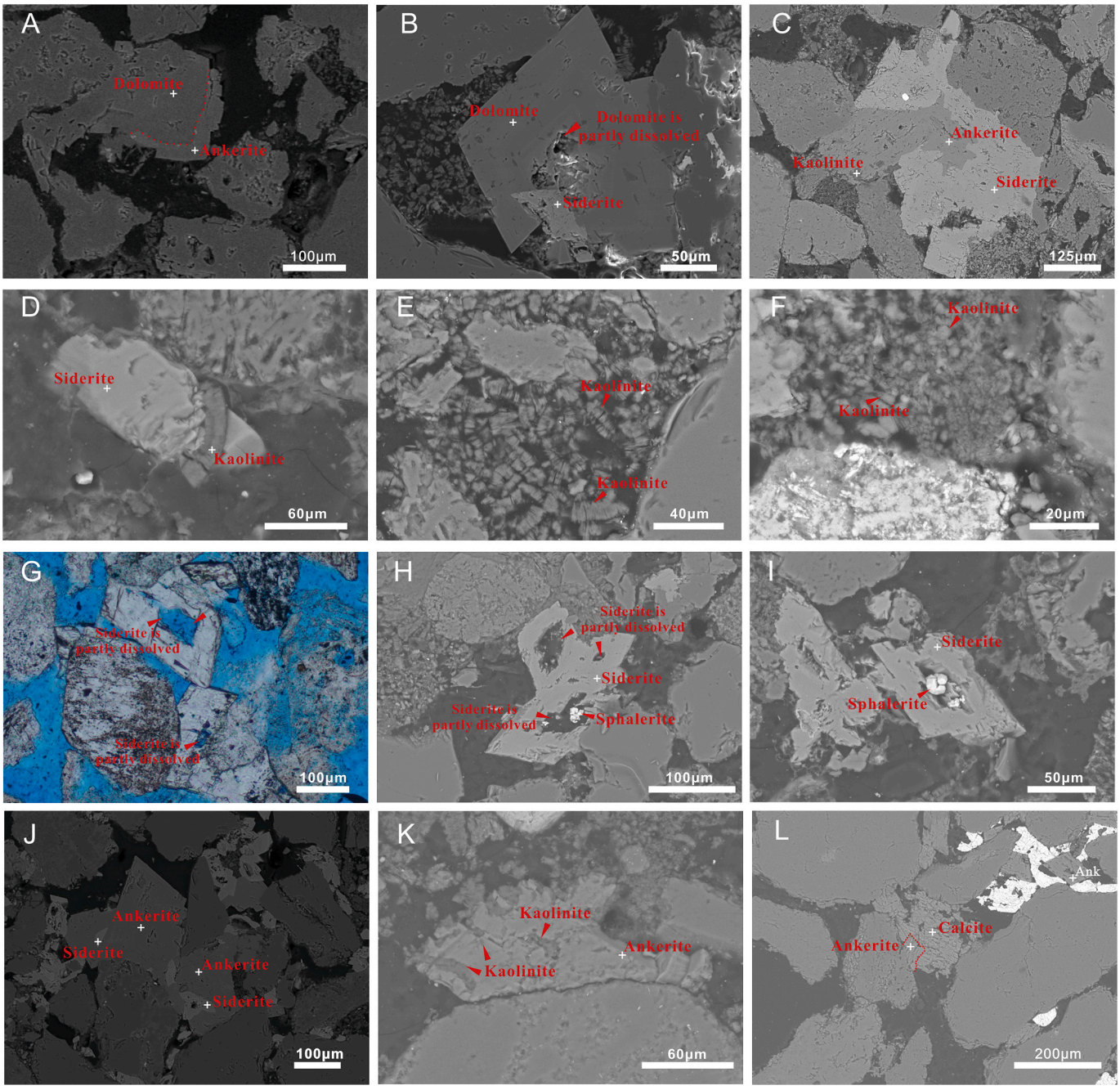


Fig. 6. (A) Dolomite is coated with ankerite in the grey sandstones near the diabase dikes; sample QC14-54A. (B) Siderite penetrates into dolomite, and dolomite is partly dissolved in the grey sandstones near the diabase dikes; sample QC29-38A. (C) Ankerite surrounds kaolinite and penetrates into siderite in the grey sandstones near the diabase dikes; sample QC19-34. (D) Vermicular kaolinite cut through siderite in the grey sandstones near the diabase dikes; sample 4109-09. (E) Vermicular and book kaolinites are distributed among detrital grains in the grey sandstones near the diabase dikes; sample 0905-18. (F) Finely granular kaolinites with different sizes occur among detrital grains in the grey sandstones far away the diabase dikes; sample QC17-47. (G) Cement dissolved pores; siderite is partly dissolved and the blue parts are pores in the grey sandstones near the diabase dikes; sample Qc19-58. (H) Siderite is partly dissolved and some of dissolved pores are filled by sphalerite in the grey sandstones near the diabase dikes; sample Qc19-25. (I) Sphalerite fills in dissolved pores of siderites in the grey sandstones near the diabase dikes; sample Qc19-25. (J) Siderite is surrounded by ankerite in the grey sandstones near the diabase dikes; sample 09-05-6A. (K) Ankerite surrounds vermicular kaolinite in the grey sandstones near the diabase dikes; sample QC14-31. (L) Calcite surrounds ankerite in the grey sandstones near the diabase dikes; sample QC19-19. The photomicrograph in Fig. 6G was taken under plane light, and the others were back-scattered electron images. (For interpretation of the references to color in this figure legend, the reader is referred to the Web version of this article.)

GeolasPro laser ablation system that consists of a COMPexPro 102 ArF excimer laser (wavelength of 193 nm and maximum energy of 200 mJ) and a MicroLas optical system. An Agilent 7700e ICP-MS instrument was used to acquire ion-signal intensities. Helium was applied as a carrier gas. Argon was used as the make-up gas and mixed with the carrier gas via a T-connector before entering the ICP. A "wire" signal smoothing device is included in this laser ablation system (Hu et al., 2015). The spot size and frequency of the laser were set to 44 μm and 5 Hz, respectively, in this study. Trace element compositions of minerals were calibrated against various reference materials (BHVO-2G, BCR-2G and BIR-1G) without using an internal standard (Liu et al., 2008). Each analysis incorporated a background acquisition of approximately 20–30 s

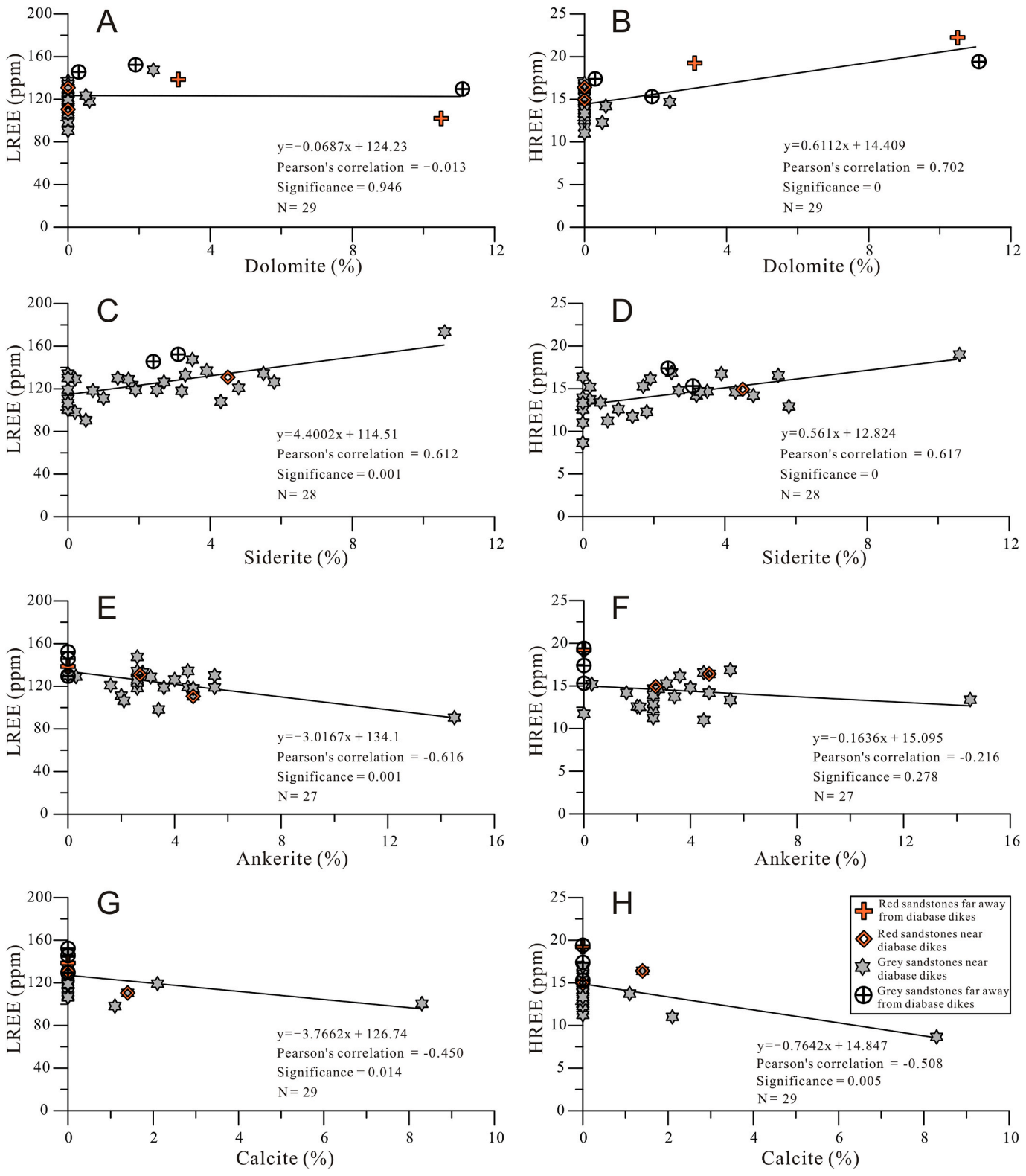


Fig. 7. (A) Cross-plot of dolomite content against LREE. (B) Cross-plot of dolomite content against HREE. (C) Cross-plot of siderite content against LREE. (D) Cross-plot of siderite content against HREE. (E) Cross-plot of ankerite content against LREE. (F) Cross-plot of ankerite content against HREE. (G) Cross-plot of calcite content against LREE. (H) Cross-plot of calcite content against HREE. (See the same legend in Fig. 7H.)

followed by 50 s of data acquisition from the sample. An Excel-based software ICPMSDataCal was used to perform off-line selection and integration of background and analyzed signals, time-drift correction and quantitative calibration for trace element analysis (Liu et al., 2008).

4. Results

4.1. REE mobility of the sandstones

The ∑LREE content ranges from 90.52 ppm to 181.20 ppm with an

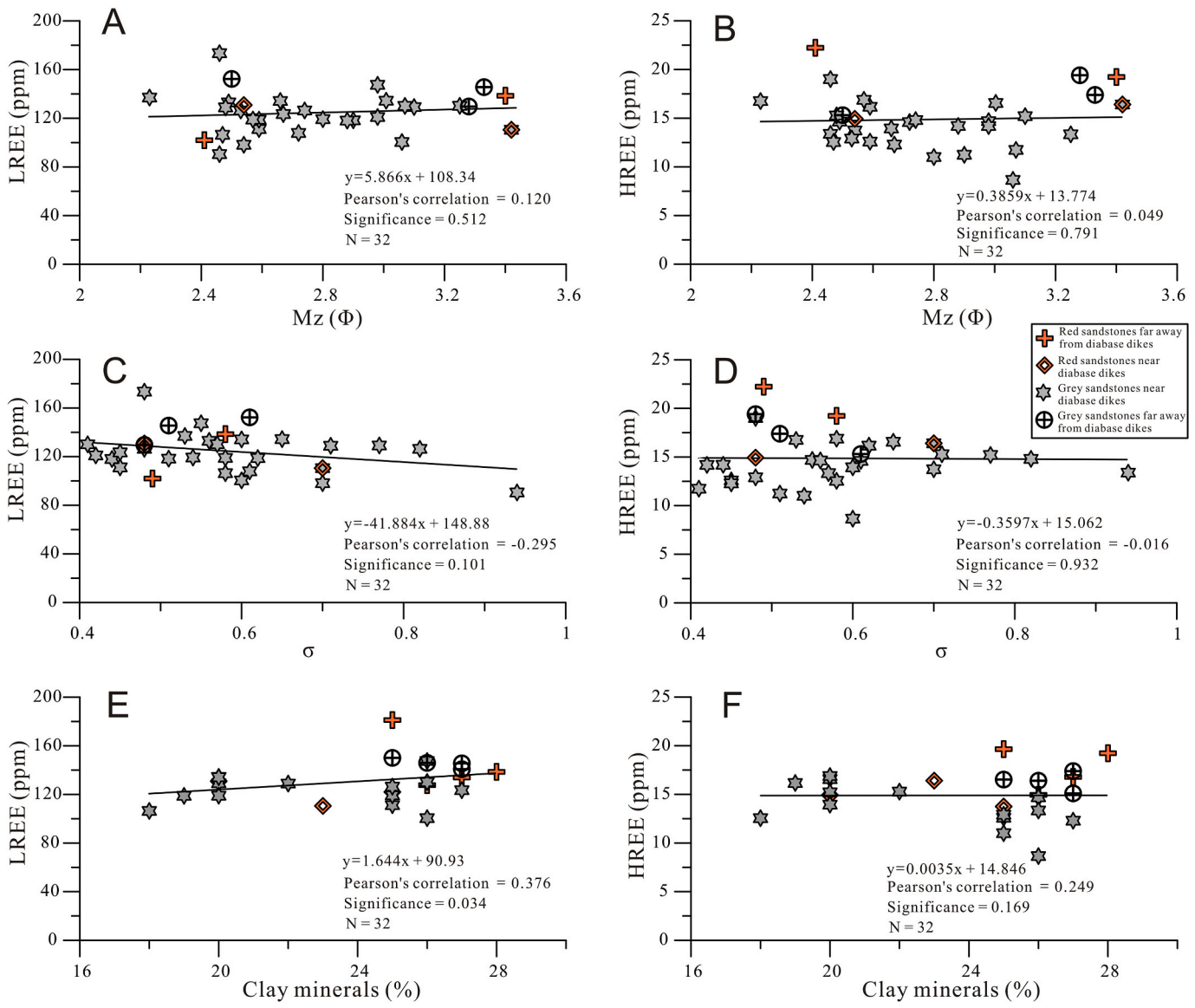


Fig. 8. (A) Cross-plot of median grain diameter against LREE. (B) Cross-plot of median grain diameter against HREE. (C) Cross-plot of standard deviation against LREE. (D) Cross-plot of standard deviation against HREE. (E) Cross-plot of clay content against LREE. (F) Cross-plot of clay content against HREE. (See the same legend in Fig. 8D.)

average of 130.38 ppm (Table 1S (Supplementary Material)). Average values of the ∑LREE content of the sandstones near the diabase dikes are lower than that of the sandstones far away from the diabase dikes (Figs. 3 and 4). Average value of the ∑HREE content with a range between 8.66 ppm and 19.65 ppm is 14.99 ppm (Table 1S (Supplementary Material)). Average values of the ∑HREE content of the sandstones near the diabase dikes are also lower than that of the sandstones far away from the diabase dikes (Figs. 3 and 4). Ratio of ∑LREE/∑HREE ranges between 6.68 and 11.60 (average 8.80), and ratio of La_N/Yb_N is 8.31–22.84 (average 12.14) (Table 1S (Supplementary Material)). Ratios of La_N/Sm_N and Gd_N/Yb_N are 3.18–6.34 (average 4.55) and 1.14–2.70 (average 1.79) respectively (Table 1S (Supplementary Material)). Chondrite-normalized REE patterns of the sandstones are characterized by distinct enrichments of the LREEs, and flat distribution of the HREEs, with negative Eu anomalies (Fig. 5A, B, C, D).

Compared with the sandstones far away from the diabase dikes, the sandstones near the diabase dikes are obviously depleted in REEs (Figs. 3 and 5A, B, C, D). The ∑LREE content, ∑HREE content and REE content are all positively correlated with the distance away from the diabase dikes, and they all increase with an increase of the distance away from the diabase dikes (Fig. 5E, F, G). Significance of the P test for these trends is less than 0.01 (Fig. 5E, F, G), indicating that these correlations are statistically valid. The ∑LREE/∑HREE is less correlated with the distance away from the diabase dikes (Fig. 5H). Fluctuation of the ∑LREE/∑HREE is apparent at a given distance away from the diabase dikes of less than 20m, while it is not pronounced at a given distance away from the diabase dikes of more than 20m (Fig. 5H). So, REE variations of the sandstones with the distance away from the diabase dikes show that REE mobility of the sandstones may be related to the diabase dikes.

4.2. Carbonate cements of the sandstones

4.2.1. Occurrence of the carbonate cements

Carbonate cements in the sandstones comprise of dolomite, siderite, ankerite and calcite. The dolomite presents as an idiomorphic granular texture with a diameter of 50–200 μm or a colloidal texture (Fig. 6A and B), and mainly distributed among detrital grains in the red and grey sandstones (Table 2S (Supplementary Material)). The dolomite tends to be partly dissolved in the sandstones near the diabase dikes (Figs. 3, 4

and 6B), and has the highest average content of 4.5% in the red sandstones far away from the diabase dikes (Fig. 4). The siderite is frequently distributed among detrital grains in the grey sandstones and sporadically found in the red sandstones (Fig. 6C and D; Table 2S (Supplementary Material)). Three types of kaolinite occur among detrital grains in the sandstones: vermicular kaolinite, book kaolinite, and finely granular kaolinite (Fig. 6D, E, F), and the former two are mainly found in the sandstones near the diabase dikes (Fig. 6D and E) while the latter is primarily distributed in the sandstones far away from the diabase dikes (Fig. 6F). Some siderites are cut through by the vermicular kaolinite (Fig. 6D), or are partly dissolved in the sandstones near the diabase dikes (Fig. 6G, H, I), resulting in formation of pores which are often filled by sphalerites or calcites. The siderite is peaking its average content of 2.8% in the grey sandstones far away from the diabase dikes (Fig. 4). The ankerite frequently has a colloidal shape or a mosaic granular structure with the highest average content of 3.7% and 3.4% in the red and grey sandstones near the diabase dikes respectively (Figs. 3, 4 and 6C, J, K, L; Table 2S (Supplementary Material)). The ankerite surrounds vermicular kaolinite (Fig. 6K). The calcite distinguished by mosaic granular texture is sporadically distributed among detrital grains in the sandstones (Figs. 3, 4 and 6L; Table 2S (Supplementary Material)).

4.2.2. REE geochemistry of the carbonate cements

The ΣLREE and ΣHREE are both decreasing in turn from the dolomite with an average value of 217.27 ppm and 232.12 ppm respectively, to the siderite with an average value of 148.94 ppm and 61.36 ppm respectively, to the ankerite with an average value of 82.12 ppm and 20.25 ppm respectively, and to the calcite with an average value of 53.62 ppm and 8.41 ppm respectively (Table 3S (Supplementary Material)). Chondrite-normalized REE patterns of the carbonate cements shows that the dolomite is characterized by depletion of LREEs and enrichment of HREEs, whereas the siderite, ankerite and calcite are all distinguished by enrichments of LREEs, and flat distribution of HREEs (Fig. 5I, J, K, L). Compared with the grey sandstones far away from the diabase dikes, the dolomite and siderite are both rich in HREEs and some LREEs including Nd, Sm and Eu, and are both depleted in some LREEs including La and Ce, the ankerite is depleted in some LREEs including La, Ce, Pr and Nd, and the calcite is depleted in HREEs and LREEs (Fig. 5I, J, K, L).

4.3. Relationship between the REE mobility and carbonate cements of the sandstones

The Pearson correlation coefficient between the dolomite content and ∑LREE content is −0.013 and their significance of the P test is 0.946, showing that there is no correlation between them (Fig. 7A). The dolomite content is positively correlated with ∑HREE content, and the general trend observed is as expected an increase of ∑HREE content as the dolomite content increases (Fig. 7B). The siderite content is positively correlated with ∑LREE content or ∑HREE content, and the general trend observed is as expected an increase of ∑LREE content or∑HREE content as the siderite content increases (Fig. 7C and D). The ankerite content is inversely correlated with ∑LREE content, and it decreases with an increase of ∑LREE content (Fig. 7E). Significance of the P test for these trends is no more than 0.001 (Fig. 7B, C, D, E), indicating that these correlations are statistically valid. There is weak correlation between the ankerite content and ∑HREE content since their Pearson correlation coefficient is −0.216, and their significance of the P test is 0.278 (Fig. 7F). The calcite content is inversely correlated with ∑LREE content or ∑HREE content, and the general trend observed is as expected a decrease of ∑LREE content or ∑HREE content as the calcite content increases (Fig. 7G and H). Significance of the P test for these trends is no more than 0.02 (Fig. 7G and H), showing that these correlations are statistically valid. Fluctuation of the ∑LREE content or ∑HREE content for a given value of the calcite content is apparent (Fig. 7G and H).

In sedimentary rocks, deposition and diagenesis are of two crucial geological factors affecting REE modification (Haley et al., 2004; Tanaka et al., 2007; Himmler et al., 2013; Soyol-Erdene and Huh, 2013; Chen et al., 2015). Median grain diameter and standard deviation of grains are used to characterize depositional textures of the sandstones. The median grain diameters of the sandstones range from 2.23 Φ to 3.53 Φ with an average value of 2.8 Φ, and the standard deviations of grains in the sandstones range from 0.41 to 0.94 with an average value of 0.57 (Fig. 8A, B, C, D; Table 2S (Supplementary Material)). The median grain diameter and standard deviation of grains are both rarely correlated with ∑LREE content or ∑HREE content since the absolute values of their Pearson correlation coefficients is less than 0.3, and their significance of the P test is more than 0.1 (Fig. 8A, B, C, D). Analysis of XRD

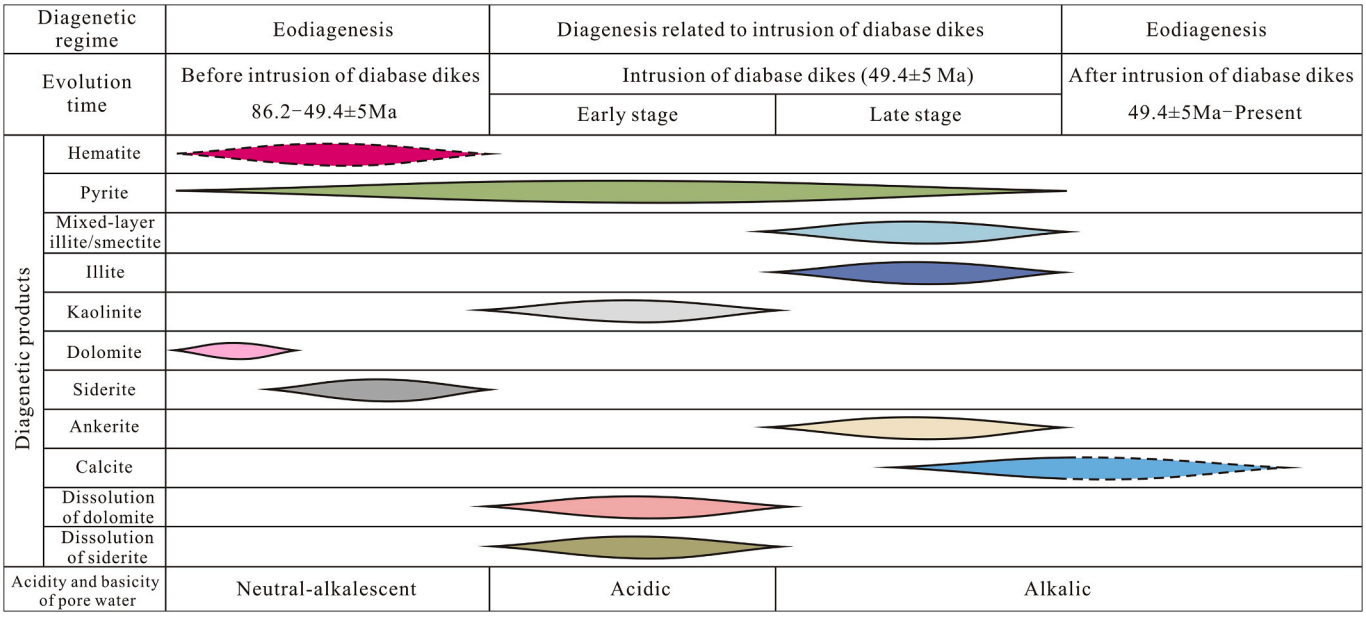


Fig. 9. Paragenetic sequence of diagenetic products in the sandstones from the Yaojia Formation in the Qianjiadian uranium deposit (Modified from Rong et al. (2016)). This figure illustrates that the dissolution of the dolomite and siderite occurred in the early stage of the diagenesis related to the intrusion of diabase dikes, and the ankerite was formed in the late stage of the diagenesis related to the intrusion of diabase dikes.

shows that interstitial materials in the sandstones of the Yaojia Formation are primarily composed of clay minerals and carbonate cements (Rong et al., 2016). In clastic sediments, clay minerals have always been considered to represent the main REE-bearing phases (Allègre and Michard, 1973; Tanaka et al., 2007). Content of the clay minerals are also weakly correlated with ∑LREE content or ∑HREE content, and fluctuation of the ∑LREE content or ∑HREE content is apparent at a given content of clay minerals (Fig. 8E and F). Thus, content of the carbonate cements may be the main geological factor affecting REE mobility of the sandstones.

5. Discussion

5.1. Effects of the diabase dikes on the carbonate cements

Carbonate cements are frequently found in sandstones near igneous intrusions (Ros, 1998; Mc Kinley et al., 2001; Grove, 2014; Liu et al., 2015; Grove et al., 2017), meanwhile they generally have variable mineral species and multiple forming stages in sandstones (Rossi et al., 2001; Beitler et al., 2005; Liu et al., 2011; Ma et al., 2016). So, the critical step evaluating effects of igneous intrusions on carbonate cements is to clarify paragenetic sequence of carbonate cements and its successive relationship with igneous intrusions. The dolomite and siderite tend to be partly dissolved in the sandstones near the diabase dikes (Figs. 3, 4 and 6B, G, H, I) and are highly accumulated in the sandstones far away from the diabase dikes (Figs. 3 and 4), indicating that dissolution of the dolomite and siderite may be related to the diabase dikes and their formation is earlier than that of the diabase dikes. The ankerite mainly occurs in the sandstones near the diabase dikes (Fig. 4), showing that formation of the ankerite could be associated with the diabase dikes. The study indicates that the dolomite, siderite, ankerite and calcite are successively formed from the early to late stage. Firstly, the dolomite is coated with the ankerite (Fig. 6A), indicating that formation of the ankerite is formed later than that of the dolomite. Secondly, the siderite penetrates into the euhedral dolomite (Fig. 6B), indicating that formation of the siderite is later than that of the dolomite. Thirdly, the vermicular kaolinite cut through the siderite, and is surrounded by the vermicular ankerite (Fig. 6D, K), indicating that formation of the vermicular kaolinite is later than that of the siderite and earlier than that of the ankerite. Fourthly, the siderite is surrounded or penetrated into by the ankerite (Fig. 6C, J), indicating that formation of the siderite is earlier than that of the ankerite. Finally, the automorphic ankerite was surrounded by the calcite (Fig. 6L), indicating that formation of the ankerite are earlier than that of the calcite.

The burial thermal evolution history of the Qianjiadian uranium deposit show that maximum burial depth of the Yaojia Formation was less than 500 m, and maximum paleotemperature was also less than 56 °C (Tian et al., 2001; Li et al., 2008). Until now there have been few reports about thermal events except the intrusion of the diabase dikes in the Qianjiadian area. So, diagenetic stages of the sandstones from the Yaojia Formation can be distinguished: eodiagenesis before the intrusion of diabase dikes, diagenesis related to the intrusion of diabase dikes, and eodiagenesis after the intrusion of diabase dikes (Fig. 9). The diagenesis related to the intrusion of diabase dikes can be further divided into two stages: the early stage is characterized by kaolinite, showing that the pore water of the sandstones is acidic, whereas the late stage is distinguished by ankerite, indicating that the pore water of the sandstones is alkalic (Fig. 9; Rong et al., 2016, 2019). The study shows that the dolomite and siderite are prone to be partly dissolved in the sandstones near the diabase dikes (Figs. 3, 4 and 6B, G, H, I). It has been generally considered that dolomite and siderite in sandstones could be dissolved by acidic pore water (Schmidt and McDonald, 1982; Surdam et al., 1989; Ma et al., 2016). So, it can be inferred that dissolution of the dolomite and siderite may occur in the early stage of the diagenesis related to the intrusion of diabase dikes.

In summary, the dissolution of the dolomite and siderite occurred in the early stage of the diagenesis related to the intrusion of diabase dikes and the ankerite was formed in the late stage of the diagenesis related to the intrusion of diabase dikes. This study indicates that the dissolution of dolomite and siderite and formation of ankerite in the sandstones are attributed to the diabase dikes, which establishes mineralogical marks for identifying sandstone reservoirs modified by igneous intrusions.

5.2. Effects of the diabase dikes on the REE mobility

The dolomite content is positively correlated with ∑HREE content, the siderite content is positively correlated with ∑LREE content or ∑HREE content (Fig. 7B, C, D), and the dissolution of the dolomite and siderite is formed in the early stage of the diagenesis related to the intrusion of diabase dikes (Fig. 9), indicating that the intrusion of diabase dikes in the early stage can result in depletion of REEs in the sandstones. The ankerite content is inversely correlated with ∑LREE content (Fig. 7E), and the ankerite was formed in the late stage of the diagenesis related to the intrusion of diabase dikes (Fig. 9), showing that the intrusion of diabase dikes in the late stage can lead to depletion of LREEs in the sandstones. In order to quantitatively illustrate effects of the diabase dikes on the REE mobility of sandstones, a theoretical model is designed. According to effects of the diabase dikes on the carbonate cements (Fig. 4), it is supposed that 4.5% dolomite and 0.5% siderite in the sandstones were dissolved, and 3.5% ankerite was formed because of intrusion of the diabase dikes. The ∑LREE content and ∑HREE content in the sandstones not affected by the diabase dikes are 146.14 ppm and 17.25 ppm respectively (Table 1S (Supplementary Material)). The ΣLREE and ΣHREE in the dolomite have an average value of 217.27 ppm and 232.12 ppm respectively, in the siderite have an average value of 148.94 ppm and 61.36 ppm respectively, and in the ankerite have an average value of 82.12 ppm and 20.25 ppm respectively (Table 3S (Supplementary Material)). It can be calculated that ∑LREE content and ∑HREE content in the sandstones affected by the diabase dikes are 140.60 ppm and 7.32 ppm respectively, and intrusion of the diabase dikes theoretically results in the decrease of ∑LREE content and ∑HREE content by 3.8% and 57.6% respectively. Thus, dissolution of the dolomite and siderite and formation of the ankerite can lead to REE depletion in the sandstones from the Qianjiadian uranium deposit.

To sum up, the mechanism of the REE depletion in the sandstones can be demonstrated that dissolution of the dolomite and siderite and formation of the ankerite were aroused by the intrusion of diabase dikes, resulting in the sandstones near the diabase being depleted in REEs. This study indicates that the depletion of REEs in the sandstones are attributed to the diabase dikes, which establishes geochemical marks for identifying sandstone reservoirs modified by igneous intrusions.

5.3. Implications for the uranium mineralization

Formation of sandstone-hosted uranium deposits is generally considered to be closely related to supergene fluids from basin margins and their mineralized temperature is relatively low (<70 °C) (Granger and Warren, 1979; Finch and Davis, 1985; Adams, 1991; Min et al., 2005; Cai et al., 2007; Jiang et al., 2012; Bonnetti et al., 2015, 2017; Hall et al., 2017). Some studies have shown that REEs are prone to move out from oxidized sandstones and deposit in mineralized sandstones in typical sandstone-hosted uranium deposits (Wang et al., 2000; Chen et al., 2007; Xue et al., 2010).

In this study, uranium mineralization occurs in the grey sandstones near the diabase dikes (Figs. 1C and 3), which can be divide into three types according to their uranium contents: mineralized grey sandstones with high grade (U > 100 ppm), mineralized grey sandstones with low grade (20 ppm < U < 100 ppm), and non-mineralized grey sandstones (U < 20 ppm). Compared with the grey sandstones far away from the diabase dikes, the mineralized grey sandstones with high grade, mineralized grey sandstones with low grade, and non-mineralized grey sandstones are depleted in REE, and their depletion degree decreases in

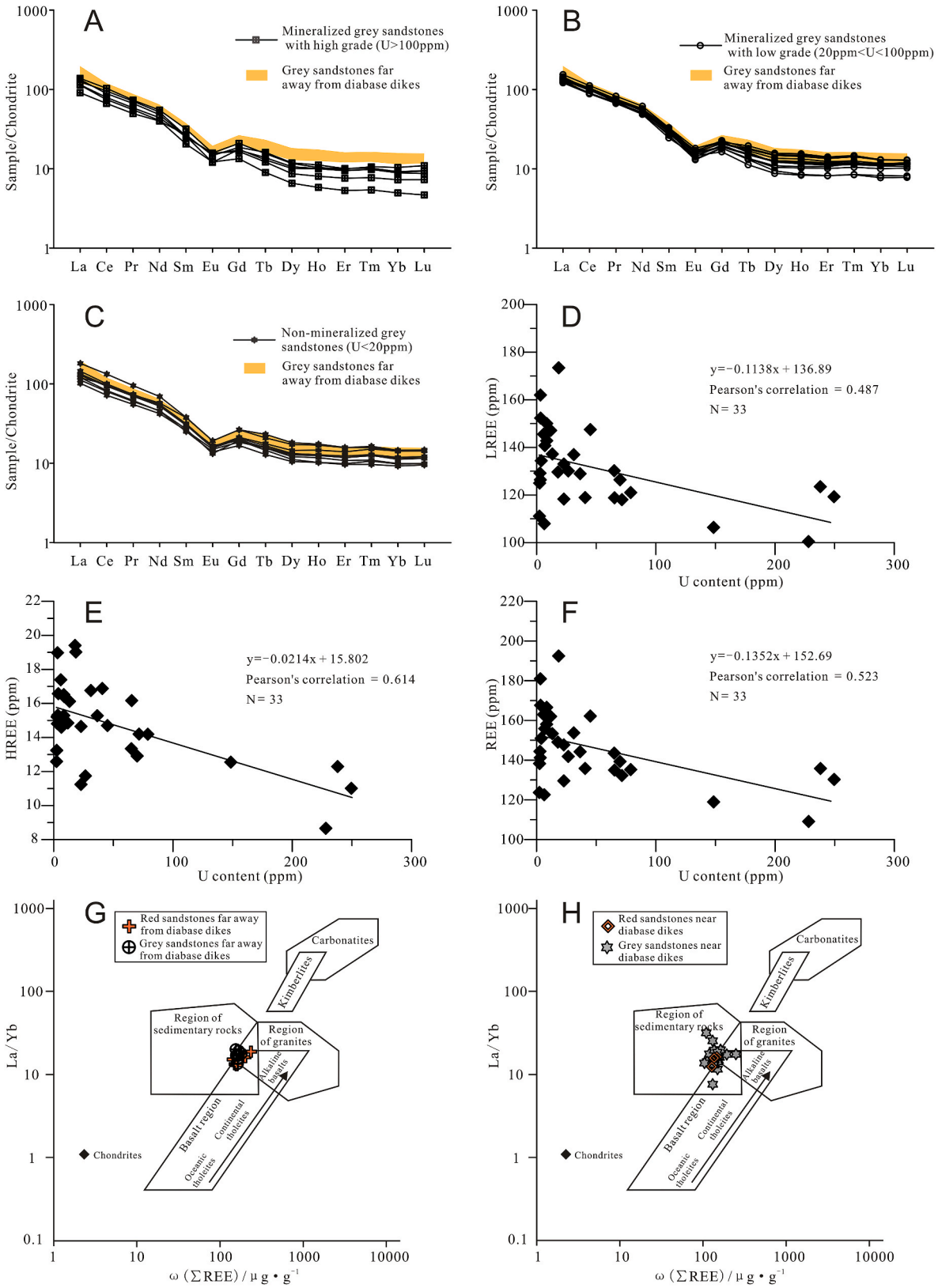


Fig. 10. (A) Chondrite-normalized REE patterns of the mineralized grey sandstones with high grade (U > 100 ppm) near the diabase dikes. (B) Chondrite-normalized REE patterns of the mineralized grey sandstones with low grade (20 ppm < U < 100 ppm) near the diabase dikes. (C) Chondrite-normalized REE patterns of the non-mineralized grey sandstones near the diabase dikes. (D) Cross-plot of U content against LREE of the grey sandstones. (E) Cross-plot of U content against HREE of the grey sandstones. (F) Cross-plot of U content against REE of the grey sandstones. (G) The ω (∑REE)-La/Yb diagram of the red and grey sandstones far away from diabase dikes. (H) The ω (∑REE)-La/Yb diagram of the red and grey sandstones near the diabase dikes. Refer to Table 1S (Supplementary Material) for detailed data. Chondrite normalizing values are from Sun and McDonough (1989). Criterion for discrimination of provenance by the ω (∑REE)-La/Yb diagram is after Allègre and Michard (1973). (For interpretation of the references to color in this figure legend, the reader is referred to the Web version of this article.)

turn (Fig. 10A, B, C). The U content is inversely correlated with ∑LREE content, ∑HREE content or ∑REE content, and the general trend observed is as expected a decrease of ∑LREE content, ∑HREE content or ∑REE content as the U content increases (Fig. 10D, E, F). Therefore, it can be inferred that the mineralization is associated with REE depletion in the sandstones of the Qianjiadian uranium deposits, significantly different from behaviors of REEs in typical sandstone-hosted uranium deposits. Consequently, the REE depletion of the sandstones will be a new prospecting indicator for the Qianjiadian uranium deposit in the Songliao Basin. This study has shown that the depletion of REEs in the sandstones is attributed to the diabase dikes. Hence, it suggests that the uranium mineralization, especially high-grade uranium mineralization could be attributed to the diabase dikes.

5.4. Implications for the tracer of sandstone provenance

REEs have always been considered as indicators of sandstone provenance in sedimentary basins since these elements are stable in geological processes (Bhatia, 1985; Verma and Armstrong-Altrin, 2013, 2016), but many studies have shown that abundance and pattern of REEs may significantly be changed during hydrothermal alteration and weathering processes (Hole et al., 1992; Wood and Williams-Jones, 1994; Cuney and Mathieu, 2000). Therefore, it is very important to quantitatively evaluate REE mobility before tracing sandstone provenance by REEs. Although REE mobility may affect discrimination of sandstone provenance by REEs, there are still few studies about evaluating their affecting degree. This study indicate that REE mobility of the sandstones occur since dissolution of the dolomite and siderite and formation of the ankerite were aroused by the intrusion of diabase dikes in the Qianjiadian uranium deposit. So, the Qianjiadian uranium deposit provide a good example for evaluating degree of the effects of REE mobility on the tracer of sandstone provenance.

The ω (∑REE)-La/Yb diagram has frequently been used to discrimination of sandstone provenance (Allègre and Michard, 1973). The ω (∑REE)-La/Yb diagram of the red and grey sandstones far away from the diabase dikes shows that parent rocks of the Yaojia Formation are complexes of sedimentary rocks, alkaline basalts, and granites (Fig. 10G). The ω (∑REE)-La/Yb diagrams of the red sandstones far away from the diabase dikes are almost overlapping with that of the grey sandstones far away from the diabase dikes (Fig. 10G), indicating that the oxidation has few effects on the tracer of sandstone provenance by REE. The ω (∑REE)-La/Yb diagram of the red and grey sandstones near the diabase dikes are apparently separated with that of the red and grey sandstones far away from the diabase dikes (Fig. 10H), revealing that the intrusion of the diabase dikes have effects on the tracer of sandstone provenance. The study shows that dissolution of the dolomite and siderite and formation of the ankerite aroused by the intrusion of diabase dikes have resulted in the sandstones near the diabase being depleted in REEs, which could cause errors during study sandstone provenance by REEs. So, the results indicate that sandstones affected by igneous intrusions should be avoided during sampling for sandstone provenance by REEs, which will provide some useful information about the tracer of sandstone provenance.

6. Conclusions

The key conclusions are summarized as follows:

(1) Compared with the sandstones far away from the diabase dikes, the sandstones near the diabase dikes are obviously depleted in REEs. ∑LREE content, ∑HREE content and REE content are all positively correlated with distance away from the diabase dikes, and they all increase with an increase of the distance away from the diabase dikes.
(2) Carbonate cements in the sandstones comprise of dolomite, siderite, ankerite and calcite, which are successively formed from the early to late stage. The dolomite and siderite tend to be partly dissolved in the sandstones near the diabase dikes, the ankerite is mainly accumulated in the sandstones near the diabase dikes, and the calcites are sporadically distributed in the sandstones. ΣLREE and ΣHREE contents are both gradually decreasing in turn from the dolomite, to siderite, to ankerite, and to calcite. The dolomite is characterized by depletion of LREEs and enrichment of HREEs, whereas the siderite, ankerite and calcite are all distinguished by enrichments of LREEs, and flat distribution of HREEs.
(3) Dolomite content is rarely correlated with ∑LREE content, but is positively correlated with ∑HREE content. Siderite content is positively correlated with ∑LREE content or ∑HREE content. Ankerite content is inversely correlated with ∑LREE content and rarely correlated with ∑HREE content. Calcite content is inversely correlated with ∑LREE content or ∑HREE content. Median grain diameter, standard deviation of grains and content of clay minerals are all rarely correlated with ∑LREE content or ∑HREE content.
(4) The dissolution of the dolomite and siderite occurred in the early stage of the diagenesis related to the intrusion of diabase dikes, and the ankerite was formed in the late stage of the diagenesis related to the intrusion of diabase dikes. Dissolution of the dolomite and siderite and formation of the ankerite were aroused by intrusion of the diabase dikes, resulting in the sandstones near the diabase dikes being depleted in REEs. High-grade uranium mineralization may be attributed to the diabase dikes, and REE depletion of the sandstones can be severe as a new prospecting indicator. Sandstones affected by igneous intrusions should be avoided during sampling for sandstone provenance by REEs.

Declaration of competing interest

We declare that we have no financial and personal relationships with other people or organizations that can inappropriately influence our work, there is no professional or other personal interest of any nature or kind in any product, service or company that could be construed as influencing the position presented in or the review of the manuscript entitled “Effects of basic intrusions on REE mobility of sandstones and their geological significance: A case study from the Qianjiadian sandstone-hosted uranium deposit in the Songliao Basin”.

Acknowledgments

This research is sponsored by the National Key Research and Development Program of China (No. 2018YFC0604202), National Natural Science Foundation of China (No. 41502105), Fundamental Research Funds for the Central Universities, China University of Geosciences (Wuhan) (No. G1323511660), and Fund of Outstanding Talents in Discipline of China University of Geosciences (Wuhan) (102-162301192664). We sincerely thank Dongmin Ji, Qingchun Li and Lei Zhang in the Development Company of New Energy Sources of Liaohe Petroleum Exploration Bureau for their guidance and selfless help. We also acknowledge the efforts of Wei Gao and Hongfang Chen from Wuhan Sample Solution Analytical Technology Co., Ltd., Wuhan, China for their LA-ICP-MS experiment. Xiaojin Wang is thanked for useful discussion and language polishing.

Appendix A. Supplementary data

Supplementary data to this article can be found online at https://doi.org/10.1016/j.apgeochem.2020.104665.

References

Adams, S.S., 1991. Evolution of genetic concepts for principal types of sandstone uranium deposits in the United States. Econ. Geol. Monogr. 8, 225–248.

Allègre, C.J., Michard, G., 1973. Introduction to Geochemistry. Reidel Publishing Company, Boston, D, p. 69.
Beitler, B., Parry, W.T., Chan, M.A., 2005. Fingerprints of fluid flow: chemical diagenetic history of the Jurassic Navajo sandstone, Southern Utah, USA. J. Sediment. Res. 75, 547–561.
Bhatia, M.R., 1985. Rare earth element geochemistry of Australian Paleozoic gray wackes and mudrocks: provenance and tectonic control. Sediment. Geol. 45, 97–113.
Bonnetti, C., Cuney, M., Michels, R., Truche, L., Malartre, F., Liu, X., Yang, J., 2015. The multiple roles of sulfate-reducing bacteria and Fe-Ti oxides in the genesis of the Bayinwula roll front-type uranium deposit, Erlian Basin, NE China. Econ. Geol. 110, 1059–1081.
Bonnetti, C., Liu, X., Yan, Z., Cuney, M., Michels, R., Malartre, F., Mercadier, J., Cai, J., 2017. Coupled uranium mineralisation and bacterial sulphate reduction for the genesis of the Baxingtu sandstone-hosted U deposit, SW Songliao Basin, NE China. Ore Geol. Rev. 82, 108–129.
Brauckmann, F.J., Fuchtbauer, H., 1983. Alterations of cretaceous siltstones and sandstones near basalt contacts (Nugssaud Greenland). Sediment. Geol. 35, 193–213.
Cai, C., Dong, H., Li, H., Xiao, X., Ou, G., Zhang, C., 2007. Mineralogical and geochemical evidence for coupled bacterial uranium mineralization and hydrocarbon oxidation in the Shashagetai deposit, NW China. Chem. Geol. 236, 167–179.
Chen, J., Algeo, T.J., Zhao, L., Chen, Z., Cao, L., Zhang, L., Li, Y., 2015. Diagenetic uptake of rare earth elements by bioapatite, with an example from Lower Triassic conodonts of South China. Earth Sci. Rev. 149, 181–202.
Chen, X., Fang, X., Guo, Q., Xia, Y., Pang, Y., Sun, Y., 2008. Re-disscussion on uranium metallogenesis in qianjiadian sag, Songliao Basin. Acta Geol. Sin. 82, 553–561 (in Chinese with English abstract).
Chen, Y., Zhu, X., Zhang, C., Chen, Y., Peng, X., Wang, J., 2007. A preliminary study on REE transformation regularities of the interlayer oxidation zone in sandstone-type uranium deposit: in case of the Ili and Turpan-Hami Basins. Geol. Rev. 53, 473–485 (in Chinese with English abstract).
Chowdhury, A.H., Noble, J.P.A., 1996. Origin, distribution and significance of carbonate cements in the Albert Formation reservoir sandstones, New Brunswick, Canada. Mar. Petrol. Geol. 13, 837–846.
Cuney, M., Mathieu, R., 2000. Extreme light rare earth element mobilization by diagenetic fluids in the geological environment of the Oklo natural reactor zones, Franceville basin. Gabon Geol. 28, 743–746.
Du, X., Xie, X., Lu, Y., Ren, J., Zhang, S., Lang, P., Cheng, T., Su, M., Zhang, C., 2011. Distribution of continental red paleosols and their forming mechanisms in the late cretaceous Yaojia Formation of the Songliao Basin, NE China. Cretac. Res. 32, 244–257.
Einsele, G., Gieskes, J.M., Curray, J., Moore, D.M., Aguayo, E., Aubry, M.P., Fornari, D., Guerrero, J., Kastner, M., Kelts, K., Lyle, M., Matoba, Y., Molina-Cruz, A., Niemitz, J., Rueda, J., Saunders, A., Schrader, H., Simoneit, B., Vacquier, V., 1980. Intrusion of basaltic sills into highly porous sediments, and resulting hydrothermal activity. Nature 283, 441–445.
Fang, S., Zhang, Z., Liu, Z., Dong, Q., Wan, J., Du, J., 2007. Hydrothermal history and stratum age in the Cenozoic of the Songliao Basin, NE China. J. Jilin Univ. (Earth Sci. Ed.) 37, 923–928 (in Chinese with English abstract).
Feng, Z., Jia, C., Xie, X., Zhang, S., Feng, Z., Cross, T.A., 2010. Tectonostratigraphic units and stratigraphic sequences of the nonmarine Songliao basin, northeast China. Basin Res. 22, 79–95.
Finch, W.I., Davis, J.F., 1985. Sandstone-type uranium deposits: an introduction. In: Geological Environments of Sandstone-type Uranium Deposits. Vienna, IAEA-TECDOC-38, pp. 11–20.
Folk, R.L., Ward, W.C., 1957. Brazos River Bar [Texas]: a study in the significance of grain size parameters. J. Sediment. Petrol. 27, 3–26.
Friedman, G.M., 1958. Determination of sieve-size distribution from thin-section data for sedimentary petrological studies. J. Geol. 66, 394–416.
Friedman, G.M., 1962. Comparison of moment measure for sieving and thin-section data in sedimentary petrological studies. J. Sediment. Petrol. 32, 15–25.
Girard, J.P., Nahon, D., 1989. Diagenesis of the upper Proterozoic siliciclastic sediments of the Taoudeni Basin (West Africa) and relation to diabase emplacement. J. Sediment. Petrol. 59, 233–248.
Granger, H.C., Warren, C.G., 1979. The Importance of Dissolved Free Oxygen During Formation of Sandstone Type Uranium Deposits, 79–1603. U.S. Geological Survey, p. 22. Open file Report.
Grove, C., 2014. Direct and Indirect Effects of Flood Basalt Volcanism on Reservoir Quality Sandstone. Ph.D. theses. Durham University, Durham, England, 478pp.
Grove, C., Jerram, D.A., Gluyas, J.G., Brown, R.J., 2017. Sandstone diagenesis in sediment–lava sequences: exceptional examples of volcanically driven diagenetic compartmentalization in dune valley, huab outliers, NW Namibia. J. Sediment. Res. 87, 1314–1335.
Haley, B.A., Klinkhammer, G.P., Mcmanus, J., 2004. Rare earth elements in pore waters of marine sediments. Geochem. Cosmochim. Acta 68, 1265–1279.
Hall, S.M., Mihalasky, M.J., Tureck, K.R., Hammarstrom, J.M., Hannon, M.T., 2017. Genetic and grade and tonnage models for sandstone-hosted roll-type uranium deposits, Texas Coastal Plain, USA. Ore Geol. Rev. 80, 716–753.
Himmler, T., Haley, B.A., Torres, M.E., Klinkhammer, G.P., Bohrmann, G., Peckmann, J., 2013. Rare earth element geochemistry in cold-seep pore waters of Hydrate Ridge, northeast Pacific Ocean. Geo Mar. Lett. 33, 369–379.
Hole, M.J., Trewin, N.H., Still, J., 1992. Mobility of the high field strength, rare earth elements and yttrium during late diagenesis. J. Geol. Soc. 149, 689–692. London.
Hu, Z., Zhang, W., Liu, Y., Gao, S., Li, M., Zong, K., Chen, H., Hu, S., 2015. "Wave" signal smoothing and mercury removing device for laser ablation quadrupole and multiple collector ICP-MS analysis: application to lead isotope analysis. Anal. Chem. 87, 1152–1157.
Huang, Q., Wu, H., Wan, X., He, H., Deng, C., 2011. New progress of integrated chronostratigraphy of the cretaceous in Songliao Basin. J. Stratigr. 35, 250–257 (in Chinese with English abstract).
Jia, J., Rong, H., Jiao, Y., Wu, L., Guo, X., Cao, M., Cui, Z., Tao, Z., 2018. Occurrence of carbonate cements and relationship between carbonate cementation and uranium mineralization of Qianjiadian uranium deposit, Songliao Basin. Earth Sci. 43, 149–161 (in Chinese with English abstract).
Jiang, L., Cai, C., Zhang, Y., Mao, S., Sun, Y., Li, K., Xiang, L., Zhang, C., 2012. Lipids of sulfate reducing bacteria and sulfur-oxidizing bacteria found in the Dongsheng uranium deposit. Chin. Sci. Bull. 57, 1311–1319.
Jiao, Y., Wu, L., Peng, Y., Rong, H., Ji, D., Miao, A., Li, H., 2015. Sedimentary-tectonic setting of the deposition-type uranium deposits forming in the Paleo-Asian tectonic domain, North China. Earth Sci. Front. 22, 189–205 (in Chinese with English abstract).
Kantorowicz, J.D., Bryant, I.D., Dawans, J.M., 1987. Controls on the Geometry and Distribution of Carbonate Cements in Jurassic Sandstones: Bridport Sands, Southern England and Viking Group, Troll Field, Norway, vol. 36. Geological Society of London Special Publications, pp. 103–118.
Lai, J., Li, D., Wang, G., Xiao, C., Cao, J., Wu, C., Han, C., Zhao, X., Qin, Z., 2019. Can carbonate cementation be inhibited in continental red bed sandstone? J. Petrol. Sci. Eng. 179, 1123–1135.
Li, H., Wu, S., Cai, C., Luo, X., 2008. Forming processes of petroleum-related Sandstone-type uranium ore: example from Qianjiadian uranium deposit. Geochimica 37, 523–532 (in Chinese with English abstract).
Liu, C., Xie, Q., Wang, G., Cui, Y., Zhang, C., 2015. The influence of igneous intrusion to detrital reservoir: advances and outlook. Adv. Earth Sci. 30, 654–667 (in Chinese with English abstract).
Liu, C., Zhang, S., Liu, T., Yan, Z., Guo, G., Liang, L., 2011. Chemical Composition and isotopic characteristics of the carbonate cements in sandstone reservoir layer of Dongying Sinking. Procedia Earth Planet. Sci. 2, 284–290.
Liu, S., Huang, S., Shen, Z., Lv, Z., Song, R., 2014. Diagenetic fluid evolution and water-rock interaction model of carbonate cements in sandstone: an example from the reservoir sandstone of the Fourth Member of the Xujiahe Formation of the Xiaoquan-Fenggu area, Sichuan Province, China. Sci. China Earth Sci. 57, 1077–1092.
Liu, Y., Hu, Z., Gao, S., Günther, D., Xu, J., Gao, C., Chen, H., 2008. In situ analysis of major and trace elements of anhydrous minerals by LA-ICP-MS without applying an internal standard. Chem. Geol. 257, 34–43.
Luo, Y., He, Z., Ma, H., Sun, X., 2012. Metallogenic characteristics of Qianjiadian sandstone uranium deposit in Songliao basin. Miner. Deposits 31, 391–400 (in Chinese with English abstract).
Luo, Y., Ma, H., Xia, Y., Zhang, Z., 2007. Geologic characteristics and metallogenic model of Qianjiadian uranium deposit in Songliao basin. Uranium Geol. 23, 193–199 (in Chinese with English abstract).
Ma, B., Eriksson, K.A., Cao, Y., Jia, Y., Wang, Y., Gill, B.C., 2016. Fluid flow and related diagenetic processes in a rift basin: evidence from the fourth member of the Eocene Shahejie Formation interval, Dongying depression, Bohai Bay Basin, China. AAPG Am. Assoc. Pet. Geol. Bull. 100, 1633–1662.
Mc Kinley, J.M., Worden, R.H., Ruffell, A.H., 2001. Contact diagenesis: the effect of an intrusion on reservoir quality in the triassic sherwood sandstone group, northern Ireland. J. Sediment. Res. 71, 484–495.
Mclennan, S.M., Taylor, S.R., 1979. Rare earth element mobility associated with uranium mineralization. Nature 282, 247–250.
Min, M., Chen, J., Wang, J., Wei, G., Fayek, M., 2005. Mineral paragenesis and textures associated with sandstone-hosted roll-front uranium deposits, NW China. Ore Geol. Rev. 26, 51–69.
Othman, R., Arouri, K., Warol, C.R., Mckirdy, D.M., 2001. Oil generation by igneous intrusions in the northern Gunnedah Basin, Australia. Org. Geochem. 32, 1219–1232.
Pang, Y., Chen, X., Fang, X., Sun, Y., 2010. Discussion on the interlayer oxidation and uranium metallogenesis in Qianjiadian uranium deposit, Songliao Basin. Uranium Geol. 26, 9–23 (in Chinese with English abstract).
Rong, H., Jiao, Y.Q., Wu, L.Q., Wan, D., Cui, Z.J., Guo, X.J., Jia, J.M., 2019. Origin of the carbonaceous debris and its implication for mineralization within the Qianjiadian uranium deposit, southern Songliao Basin. Ore Geol. Rev. 107, 336–352.
Rong, H., Jiao, Y., Wu, L., Ji, D., Li, H., Zhu, Q., Cao, M., Wang, X., Li, Q., Xie, H., 2016. Epigenetic alteration and its constraints on uranium mineralization from the Qianjiadian uranium deposit, southern Songliao Basin. Earth Sci. 41, 153–166 (in Chinese with English abstract).
Ros, L.F.D., 1998. Heterogeneous generation and evolution of diagenetic quartzarenites in the silurian-devonian furnas formation of the paraná basin, southern Brazil. Sediment. Geol. 116, 99–128.
Rossi, C., Marfil, R., Ramseyer, K., Permanyer, A., 2001. Facies-related diagenesis and multiphase siderite cementation and dissolution in the reservoir sandstones of the Khatatba Formation, Egypt western desert. J. Sediment. Res. 71, 459–472.
Schmidt, V., McDonald, D.A., 1982. Secondary reservoirs porosity in the course of sandstone diagenesis. AAPG Am. Assoc. Pet. Geol. Bull. 12, 4–39.
Sliwinski, M.G., Kozdon, R., Kitajima, K., Denny, A., Valley, J.W., 2016. Microanalysis of carbonate cement $\delta^{18}O$ in a CO_2-storage system seal: insights into the diagenetic history of the eau Claire formation (upper Cambrian), Illinois basin. AAPG Am. Assoc. Pet. Geol. Bull. 100, 1003–1031.
Smith, L.B., Davies, G.R., 2006. Structurally controlled hydrothermal alteration of carbonate reservoirs: an overview. AAPG Am. Assoc. Pet. Geol. Bull. 90, 1635–1640.
Soyol-Erdene, T., Huh, Y., 2013. Rare earth element cycling in the pore waters of the Bering Sea Slope (IODP Exp. 323). Chem. Geol. 358, 75–89.

Summer, N.S., Ayalon, A., 1995. Dike intrusion into unconsolidated sandstone and the development of quartzite contact zones. J. Struct. Geol. 17, 997–1010.
Sun, S., Mcdonough, W.F., 1989. Chemical and isotopic systematics of oceanic basalts: implications for mantle composition and processes. In: Saunders, A.D., Norry, M.J. (Eds.), Magmatism in the Ocean Basins, vol. 42. Geological Society of Londan, Special Publication, pp. 313–345.
Surdam, R.C., Crossey, L.J., Hagen, E.S., Heasler, H.P., 1989. Organic-inorganic interactions and sandstone diagenesis. AAPG Am. Assoc. Pet. Geol. Bull. 73, 1–23.
Tanaka, K., Akagawa, F., Yamamoto, K., Tani, Y., Kawabe, I., Kawai, T., 2007. Rare earth element geochemistry of Lake Baikal sediment: its implication for geochemical response to climate change during the Last Glacial/Interglacial transition. Quat. Sci. Rev. 26, 1362–1368.
Tian, X., Wang, G., Zou, H., 2001. Analysis of reservoir forming conditions in Hulihai sag, Qianjiadian depression. Special Oil Gas Reservoirs 8, 13–16 (in Chinese with English abstract).
Verma, S.P., Armstrong-Altrin, J.S., 2013. New multi-dimensional diagrams for tectonic discrimination of siliciclastic sediments and their application to Precambrian Basins. Chem. Geol. 355, 117–133.
Verma, S.P., Armstrong-Altrin, J.S., 2016. Geochemical discrimination of siliciclastic sediments from active and passive margin settings. Sediment. Geol. 332, 1–12.
Vincent, B., Waters, J., Witkowski, F., Daniau, G., Oxtoby, N., Crowley, S., Ellam, R., 2018. Diagenesis of Rotliegend sandstone reservoirs (offshore Netherlands): the origin and impact of dolomite cements. Sediment. Geol. 373, 272–291.
Wan, X., Zhao, J., Scott, R.W., Wang, P., Feng, Z., Huang, Q., Xi, D., 2013. Late cretaceous stratigraphy, Songliao Basin, NE China: SK1 cores. Palaeogeogr. Palaeoclimatol. Palaeoecol. 385, 31–43.
Wang, G., Hua, R., Qin, L., 2000. The role of fluids in the ore-forming process of the interlayer uranium deposits of Wukurqi district on the southern margin of Yili Basin. Miner. Deposits 19, 340–349 (in Chinese with English abstract).
Wang, Q., Hao, L., Chen, G., Zhang, G., Zhang, R., Ma, X., Wang, H., 2010. Forming mechanism of carbonate cements in siliciclastic sandstone of Zhuhai Formation in Baiyun Sag. Acta Pet. Sin. 31, 553–558.
Wang, C., Scott, R.W., Wan, X., Graham, S.A., Huang, Y., Wang, P., Wu, H., Dean, W.E., Zhang, L., 2013. Late Cretaceous climate changes recorded in Eastern Asian lacustrine deposits and North American Epieric sea strata. Earth Sci. Rev. 126, 275–299.
Wood, S.A., Williams-Jones, A.E., 1994. The aqueous geochemistry of the rare earth elements and yttrium 4. Monazite solubility and REE mobility in exhalative massive sulfide-depositing environments. Chem. Geol. 115, 47–60.
Xia, Y., Zheng, J., Li, Z., Li, L., Tian, S., 2010. Metallogenic characteristics and model of the Qianjiadian uranium deposit in the Songliao basin. Miner. Deposits 29, 154–155 (in Chinese with English abstract).
Xu, K., Li, Y., 1995. Late mesozoic strata of the Kailu basin. J. Stratigr. 19, 88–95 (in Chinese with English abstract).
Xue, W., Xue, C., Chi, G., Peng, Y., Wang, K., 2010. Trace element and REE geochemical characteristics of sandstone-type uranium deposit in the Dongsheng area of the Ordos Basin, China. Geoscience 24, 776–784 (in Chinese with English abstract).
Zhao, L., Cai, C., Jin, R., Li, J., Li, H., Wei, J., Guo, H., Zhang, B., 2018. Mineralogical and geochemical evidence for biogenic and petroleum-related uranium mineralization in the Qianjiadian deposit, NE China. Ore Geol. Rev. 101, 273–292.
Zhang, Q., Jin, W., Wang, J., Chen, W., Li, C., Jiao, S., Shao, G., 2016. Relationship between magma thermal field and hydrocarbon accumulation. Prog. Geophys. 31, 1525–1541 (in Chinese with English abstract).
Zong, K., Klemd, R., Yuan, Y., He, Z., Guo, J., Shi, X., Liu, Y., Hu, Z., Zhang, Z., 2017. The assembly of Rodinia: the correlation of early Neoproterozoic (ca. 900 Ma) high-grade metamorphism and continental arc formation in the southern Beishan Orogen, southern Central Asian Orogenic Belt (CAOB). Precambrian Res. 290, 32–48.